Arabian Journal of Geosciences (2021) 14:2645
https://doi.org/10.1007/s12517-021-08683-y

3RD CAJG 2020

Phase space study of viscous fingering and saturation pre- and post-breakthrough using lattice Boltzmann simulations of two-phase flow

Peter Mora[1] · Gabriele Morra[2] · Dave A. Yuen[3,4] · Ruben Juanes[5]

Received: 19 April 2021 / Accepted: 13 October 2021

Abstract
Viscous fingering is the occurrence of narrow fingers of an invading less viscous fluid such as water in a porous medium filled with a more viscous fluid such as oil, and its occurrence dramatically affects enhanced oil recovery by water flooding. We conduct 2D simulations using the lattice Boltzmann method for two-phase flow through a porous medium initially saturated with a fluid of a given viscosity in which a fluid of another viscosity is injected from the left side of the model. We conduct suites of simulations over viscosity ratios ($\sim 1/$(mobility ratio)) from $M = 0.01$ through $M = 100$ and for wetting angles from non-wetting to fully wetting. We plot the phase space of saturation (= Recovery Factor) versus wetting angle and viscosity ratio. We remove the dominant viscosity ratio effect to study the effect of wetting angle and find that while there is some tendency for the saturation to be higher with increasing wettability, the saturation landscape is complex with hills and valleys in which optimal wetting angles exist that maximize saturation. Furthermore, the phase space landscape is found to depend on the porous matrix geometry. We also plot saturation post-breakthrough and find that the saturation continues to increase albeit at an ever decreasing rate. This research demonstrates the potential of the lattice Boltzmann method for two-phase flow to reveal unexpected behavior and phenomena with both scientific and practical significance such as optimization of recovery factors in enhanced oil recovery (EOR).

Keywords Multiphase flow · Viscous fingering · Phase space study · Wettability · Porous media · Lattice Boltzman simulation

Introduction

When a low viscosity fluid invades a higher viscosity fluid above a critical capillary number, patterns of viscous fingering occur. Namely, narrow tendrils of the low viscosity fluid pushing into the higher viscosity fluid (Homsy 1997; Måløy et al. 1985; Chen and Wilkinson 1985; Lenormand et al. 1988). These narrow channels of the low viscosity fluid have immense significance to enhanced oil recovery (EOR) using water flooding where water is injected at an injection well with the goal of pushing out oil which is produced at an adjacent well. This is because the narrow fingers decrease the final saturation and hence the recovery factor (RF) at breakthrough when the less viscous fluid (water) reaches the production well which is when production is typically stopped. The morphology of the fingers is affected by many parameters of the fluid including the wettability and the viscosity ratio, and potentially the geometry of the porous medium. As such, the final saturation, and hence RF, at breakthrough when the invading fluid reaches the production well is a complex function of fluid properties and the geometry of the porous medium.

Numerous studies in petroleum engineering (Deng et al. 2020) have lead to a consensus that the RF increases with wettability of the invading fluid. Specifically, many core-scale experiments indicate that saturation at breakthrough (sweep) increases when the invading fluid's wettability is increased, such as by addition of surfactants or by the use of low-salinity water flooding (Kennedy et al. 1955; Jadhunandan and Morrow 1995; Seethepalli et al. 2004; Morrow and Buckley 2011; Sharma and Mohanty 2013).

Communicated by: Santanu Banerjee

This paper was selected from the 3rd Conference of the Arabian Journal of Geosciences (CAJG), Tunisia 2020.

✉ Peter Mora
wolop2008@gmail.com

Extended author information available on the last page of the article.

Published online: 25 November 2021

This paper makes use of the lattice Boltzmann method (LBM) for two-phase flow (Rothman and Keller 1988; Gunstensen et al. 1991; Latva-Kokko and Rothman 2005; Reis and Phillips 2007; Mora et al. 2021) to study the effect of wetability, viscosity ratio, and porous medium geometry on the sweep as a function of viscosity ratio and wetting angle. Specifically, we extend previous work (Mora et al. 2021) where we found that the effect wettability on saturation at breakthrough was complex, and demonstrated that the saturation did not necessarily increase with wettability, and that optimal wetting angles $\theta_w > 0$ that maximized saturation (sweep) could occur at specific viscosity ratios. Here, we aim to study the effect of flow morphology and pore matrix geometry on sweep as a function of wetting angle and viscosity ratio ($\sim 1/(\text{mobility ratio})$) to improve understanding the complex sweep phase space. In addition, we study the evolution of saturation post-breakthrough.

Although the LBM simulations are performed in 2D due to computational limitations, we believe that the general conclusions will be applicable to the 3D case, although we caution that details will change. Ultimately, large-scale 3D simulations coupled with laboratory studies would be required to validate this expectation and ensure that the conclusions can be reliably applied in 3D.

Numerical simulation methodology

We utilize the Rothman-Keller (RK) color gradient lattice Boltzmann model to simulate two-phase flow in a simplified 2D model of a porous rock. This method was originally derived for a lattice gas (Rothman and Keller 1988; Gunstensen et al. 1991), and subsequently extended to the lattice Boltzmann method (LBM) by Latva-Kokko and Rothman (2005). This approach involves three steps which model particle distributions denoted f_α^k of two fluids (red and blue for $k = 1$ and $k = 2$) moving in the α-direction on a discrete lattice. Namely, (1) streaming (movement), (2) collision, and (3) recoloring.

The macroscopic density of the two fluids is given by

$$\rho_k = \sum_\alpha f_\alpha^k \quad , \tag{1}$$

the total density of the fluid is given by

$$\rho = \sum_k \rho_k \quad , \tag{2}$$

the momentum of the fluid is given by

$$\rho \mathbf{u} = \sum_k \sum_\alpha f_\alpha^k \mathbf{c}_\alpha, \tag{3}$$

and the pressure in the fluid is obtained from the equation of state and can be calculated as

$$p = c_s^2 \rho \quad . \tag{4}$$

The above equations enable the macroscopic density and velocity of the fluid ρ and $\mathbf{u}$ to be calculated from the number densities of the two fluids f_α^k.

Streaming step

The streaming step is the same as for any lattice Boltzmann method and is given by

$$f_\alpha^k(\mathbf{x}, t) = f_\alpha^k(\mathbf{x} - \mathbf{c}_\alpha \Delta t, t - \Delta t) \quad , \tag{5}$$

where $\mathbf{c}_\alpha$ is the lattice velocity vector in direction α on the lattice given by

$$\mathbf{c}_\alpha = [(0,0), (1,0), (-1,0), (0,1), (0,-1), (1,1), (-1,-1), (1,-1), (-1,1)]\Delta x/\Delta t$$

where Δt is the time step and Δx is the lattice spacing of a square lattice, namely a $D2Q9$ lattice where $D = 2$ is the number of dimensions and $Q = 9$ is the number of velocities. Using this definition, $\mathbf{c}_0$ is the null velocity, $\mathbf{c}_\alpha$ ($\alpha = 1, 2, 3, 4$) are the velocities along the coordinate axes, and $\mathbf{c}_\alpha$ ($\alpha = 5, 6, 7, 8$) are the velocities along diagonals of the lattice. In the following, we model a unitary lattice with $\Delta x = \Delta t = 1$.

Collision step

The collision step is given by Latva-Kokko and Rothman (2005)

$$f_\alpha^{k*}(\mathbf{x}, t) = f^k(\mathbf{x}, t) + \left(\Delta f_\alpha^k\right)^1 + \left(\Delta f_\alpha^k\right)^2 \quad , \tag{6}$$

where the superscript * denotes the post collision distributions.

The first collision term is nearly the same as the standard collision term of the BGK LBM (Qian et al. 1992; Chen and Doolen 1998) and is given by

$$\left(\Delta f_\alpha^k\right)^1 = \frac{1}{\tau}\left(f_\alpha^{k,eq}(\mathbf{x}, t) - f_\alpha^k(\mathbf{x}, t)\right) \tag{7}$$

where τ is the relaxation time and $f_\alpha^{k,eq}(\mathbf{x}, t)$ is the equilibrium distribution and is given by Grunau et al. (1993)

$$\begin{aligned} f_\alpha^{k,eq} &= \rho_k \left(C_\alpha^k + w_\alpha \left[\frac{\mathbf{c}_\alpha \cdot \mathbf{u}}{c_s^2} + \frac{(\mathbf{c}_\alpha \cdot \mathbf{u})^2}{2c_s^4} - \frac{\mathbf{u}^2}{2c_s^2} \right] \right) \\ &= \rho_k \left(C_\alpha^k + w_\alpha \left[3(\mathbf{c}_\alpha \cdot \mathbf{u}) + \frac{9}{2}(\mathbf{c}_\alpha \cdot \mathbf{u})^2 - \frac{3}{2}\mathbf{u}^2 \right] \right) \end{aligned} \tag{8}$$

where $c_s = \Delta x/(\sqrt{3}\Delta t) = 1/\sqrt{3}$ is the speed of sound in the lattice, and w_α are the standard LBM weights for a D2Q9 square lattice. Namely, $w_0 = 4/9$, $w_\alpha = 1/9$

for $\alpha = 1,2,3,4$ and $w_\alpha = 1/36$ for $\alpha = 5,6,7,8$. The above equilibrium distribution is identical to the standard equilibrium distribution except for the rest factor C_α (Grunau et al. 1993) instead of w_α which allows for different density fluids. The relaxation time of each fluid is related to the kinematic viscosity of each fluid through

$$\nu_k = c_s^2(\tau_k - 0.5)\Delta t \quad , \tag{9}$$

where ν_k is the kinematic viscosity of fluid k and τ_k is the relaxation time of fluid k. The relaxation time τ in Eq. (8) is interpolated at the interface between the fluids (Grunau et al. 1993) such that it changes smoothly which avoids numerical instability.

The second collision term $\left(\Delta f_\alpha^k\right)^2$ adds an attractive force between like fluids thus enabling immiscible fluids to be simulated and is given by Reis and Phillips (2007)

$$\left(\Delta f_\alpha^k\right)^2 = A|\mathbf{F}|\left(w_\alpha(\cos(\lambda_\alpha)|\mathbf{c}_\alpha|)^2 - B_\alpha\right) \quad , \tag{10}$$

where $\mathbf{F}(\mathbf{x},t)$ is the color gradient, λ_α is the angle between $\mathbf{F}(\mathbf{x},t)$ and $\mathbf{c}_\alpha$, A is a parameter that controls the interfacial tension, and B_α are coefficients given by Reis and Phillips (2007). Surface tension in the model is also affected by the two viscosities ν_1 and ν_2, and hence τ_1 and τ_2. As such, one must conduct a numerical experiment for a given set of viscosities ν_1 and ν_2 to calculate the pressure within and without a static droplet and apply the Young-Laplace formula to obtain the exact relationship between A and surface tension for the specified viscosities. The color gradient $\mathbf{F}(\mathbf{x},t)$ is calculated according to Mora et al. (2021) which optimizes isotropy of the color gradient as

$$\mathbf{F}(\mathbf{x},t) = \sum_\alpha b_\alpha \mathbf{c}_\alpha \left(\rho_1(\mathbf{x}+\mathbf{c}_\alpha\Delta t,t) - \rho_2(\mathbf{x}+\mathbf{c}_\alpha\Delta t,t)\right), \tag{11}$$

where the $\mathbf{c}_\alpha$ are the velocities and b_α are scalar coefficients of the finite difference approximation of the color gradient that is accurate to second order, namely

$$b_\alpha = \begin{cases} \frac{1}{W} & \alpha = 1,2,3,4 \\ \frac{w}{W} & \alpha = 5,6,7,8 \end{cases} \quad , \tag{12}$$

where w is the weight of the diagonal nearest neighbors relative to orthogonal nearest neighbors in the finite difference calculation of the color gradient and W is given by

$$W = 2 + 4w \quad . \tag{13}$$

The choice of w that optimizes the isotropy of the numerical color gradient depends on the interfacial thickness parameter β which will be described in the next section.

Recoloring step

The final step of the RK LBM is a "recoloring" step which achieves color segregation of the two fluids and is given by Latva-Kokko and Rothman (2005)

$$f_\alpha^1 = \frac{\rho_1}{\rho} f_\alpha^* + \beta\frac{\rho_1\rho_2}{\rho^2} f_\alpha^{eq}(\rho, \mathbf{u}=0)\cos(\lambda_\alpha) \quad , \tag{14}$$

and

$$f_\alpha^2 = \frac{\rho_2}{\rho} f_\alpha^* - \beta\frac{\rho_1\rho_2}{\rho^2} f_\alpha^{eq}(\rho, \mathbf{u}=0)\cos(\lambda_\alpha) \quad , \tag{15}$$

where $f_\alpha^* = \sum_k f_\alpha^{k*}$, $\beta \in (0,1]$ is an adjustable parameter that affects the interfacial thickness, and $f_\alpha^{eq}(\rho, \mathbf{u}=0)$ is the standard equilibrium distribution at zero velocity given by

$$f_\alpha^{eq}(\rho, \mathbf{u}=0) = w_\alpha \rho \quad . \tag{16}$$

In this paper, we use the commonly used value of $\beta = 0.5$ for the interfacial thickness parameter. As such, we use a weighting factor $w = 0.298$ (Mora et al. 2021) in Eqs. 12 and 13 which optimizes the isotropy of the color gradient at a small radius of curvature interfaces such as those that occur in flow through a porous medium.

Solid boundary conditions and wetting angle

No-slip boundary conditions are achieved in the lattice Boltzmann method by standard "bounce-back" boundary conditions at the solid interface in which number densities reflect back in the direction they came from at fluid-solid interfaces. The RK LBM model for two-phase flow allows any wetting contact angle θ_w to be specified by setting the densities of the two fluids in the solid region through (Latva-Kokko and Rothman 2005)

$$\theta_w = \cos^{-1}\left(\frac{\rho_{w1} - \rho_{w2}}{\rho_i}\right) \quad , \tag{17}$$

where ρ_{w1} is the density of fluid 1 in the solid regions, ρ_{w2} is the density of fluid 2 in the solid regions, and ρ_i is the initial density of the majority component = ρ_2. This is achieved by setting densities of the red and blue fluid in the solid regions using

$$\rho_{w1} = \rho_i\frac{1+\cos(\theta_w)}{2} \quad , \tag{18}$$

and

$$\rho_{w2} = \rho_i\frac{1-\cos(\theta_w)}{2} \quad . \tag{19}$$

The RK LBM model described above that is used in this study has been shown both theoretically and numerically to correctly model two-phase flow. Specifically, the model has been shown to yield the Navier-Stokes equations for two-phase flow (Gunstensen et al. 1991) allowing for variable density fluids (Grunau et al. 1993), variable surface tension (Reis and Phillips 2007), and any wettability (Latva-Kokko and Rothman 2005). In addition, the model has

had numerous numerical verification tests for various cases which have been summarized in Huang et al. (2015). In particular, the method has been shown to be capable of modelling the $M - Ca$ phase diagram mapping out the three domains of viscous fingering, capillary fingering, and stable displacement in a porous matrix (Huang et al. 2014) which is consistent with experimental studies such as Lenormand et al. (1988). In addition, the LBM model results and other pore-scale models for multiphase flow have been compared which demonstrates overall good performance of the LBM models to capture pore-scale multiphase flow phenomenology (Zhao et al. 2019). The above theoretical, comparative, and numerical/experimental verifications suggest that the RK LBM will at least do a reasonable job of correctly capturing two-phase flow characteristics in the current work.

Results

In the following, we aim to study the effect of wetting angle and viscosity ratio on saturation at and beyond breakthrough using 2D RK LBM simulations. We will conduct suites of runs through 2D models and measure the saturation = recovery factor at breakthrough as a function of viscosity ratio M and θ_w where $M \in [0.01, 100]$ and $\theta_w \in [0°, 180°]$. Each suite will consist of 81 simulations where we sample M in increments of $\Delta \log_{10} M = 0.5$ and θ_w in increments of $\Delta\theta_w = 22.5°$. In addition, we will conduct runs beyond breakthrough for the case of $M = 0.01$ to study whether the saturation and flow pattern continues to evolve beyond breakthrough for the non-wetting and wetting cases.

Numerical experimental setup

We initialized a square model shown in Fig. 5 consisting of 300×300 pixels by dropping random-sized circular grains with radii between $5\Delta x$ and $15\Delta x$ and accepting only those grains that are separated from other grains by at least $4\Delta x$. This leads to an unrealistically high porosity compared to 3D media but ensures the 2D granular medium has significant permeability; and hence, we will be able to model viscous fingering. The model rock matrix is initially saturated by a "blue" fluid and a "red" fluid is injected from the left boundary at a constant rate, while the pressure at the right boundary is fixed. We use Zou and He's boundary conditions (Zou and He 1997) to set the injection velocity at the left and pressure at the right of the model. Periodic boundary conditions are used at the upper and lower boundaries.

The densities of the two fluids were set to be identical and unitary so $\rho_1 = \rho_2 = 1$ since the density of water and oil is similar and as such does not play a significant role in viscous fingering. The surface tension parameter A in Eq. 10 was set such that the capillary number was high with $Ca \sim 5$ which is well above the capillary to viscous fingering transition. Namely, the capillary number is defined as

$$Ca = \frac{\mu_r u_{in}}{\sigma} = \frac{\rho_r \nu_r u_{in}}{\sigma} \quad , \tag{20}$$

and relates to the relative effect of viscous drag forces versus surface tension or capillary forces where μ_r is the dynamic viscosity of the invading fluid, ν_r is the kinematic viscosity of the invading fluid, ρ_r is the density of the invading fluid, u_{in} is the injection rate, and σ is the surface tension. The value of A in the RK LBM given by Eq. 10 has been found to relate to the surface tension as

$$\sigma = \alpha A \quad , \tag{21}$$

where $\alpha \in [0.5, 2]$ over a wide range of viscosities of the two fluids ν_r and ν_b. The value of α above for a given set of viscosities ν_r and ν_b can be calculated via numerical simulation of a droplet through the Young-Laplace formula

$$\sigma = \frac{\Delta P}{r_0} = \frac{P_{in} - P_{out}}{r_0} \quad , \tag{22}$$

where ΔP is the difference in pressure inside versus outside a droplet of radius r_0.

In our experiments, we also wish to ensure slow enough flow rates such that inertial effects and turbulence are negligible. This can be achieved by specifying a low enough Reynolds number which is a dimensionless quantity which is defined as

$$Re = \frac{uL}{\nu} \quad , \tag{23}$$

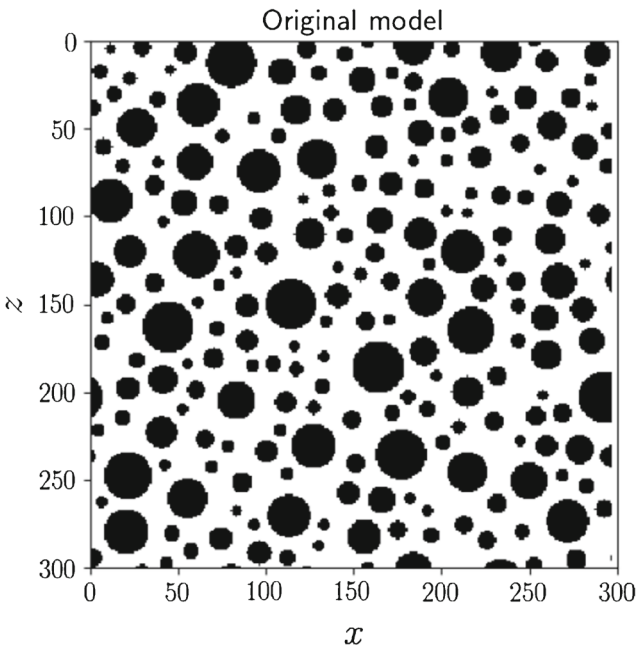

Fig. 1 The original model porous rock matrix (model 1)

where L is the scale length, ν is the kinematic viscosity, and u is the flow speed. In the following experiments, we set the injection flow rate u_{in} such that $Re = 0.2$ for an assumed scale length of $L = 4$ which is the smallest width between grains in the solid matrix. Hence, we have $Re = 0.2 \ll Re_{turbulence} \sim 2300$ which ensures inertial effects and turbulence are negligible. Using $Re = 0.2$ in Eq. 23, we have

$$u_{in} = \frac{Re \min(\nu_r, \nu_b)}{D} = \frac{0.2 \min(\nu_r, \nu_b)}{D} = 0.05 \min(\nu_r, \nu_b) \quad . \tag{24}$$

The viscosities for the simulations ν_r and ν_b must be specified to cover a wide range of viscosity ratios $M \in [0.01, 100]$ such that the RK color gradient simulations are stable and accurate. To achieve this, we choose the product of the viscosities to be $\nu_r \nu_b = (0.2)^2$ and hence we have

$$\nu_r \nu_b = M \nu_b^2 = 0.2^2 \Rightarrow \nu_b = \sqrt{0.2^2/M} \text{ and } \nu_r = M \nu_b. \tag{25}$$

From Eqs. 24 and 25, we can see that for the case of $M = 0.01$ and $M = 100$ which has $\min(\nu_r, \nu_b) = 0.02$, we will have an injection velocity $u_{in} = 0.001$, and for the

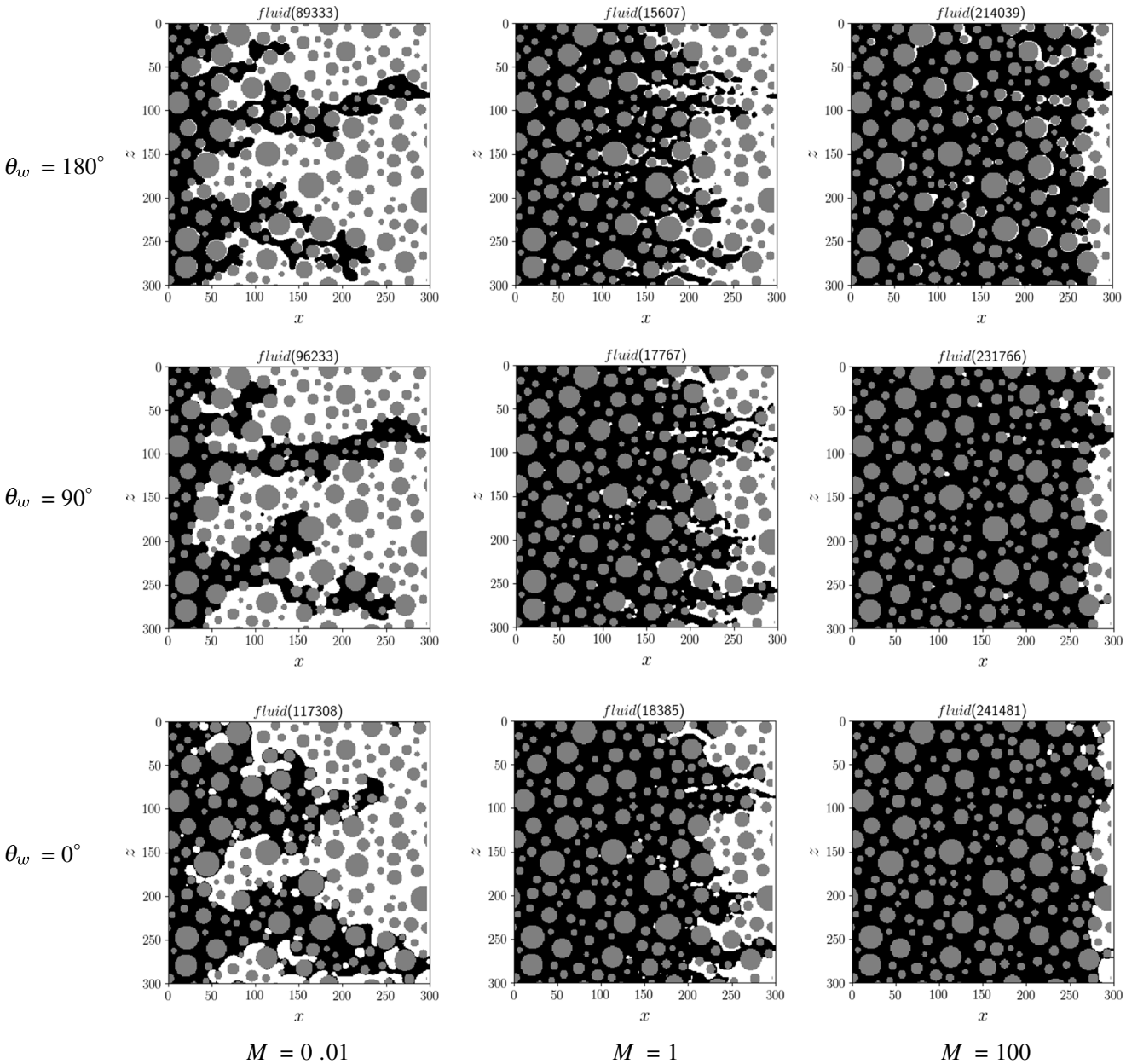

Fig. 2 Snapshots of flow patterns at the moment of breakthrough for several viscosity ratios M and wetting angles θ_w. The black region indicates the red invading fluid and the white area is the defending blue fluid

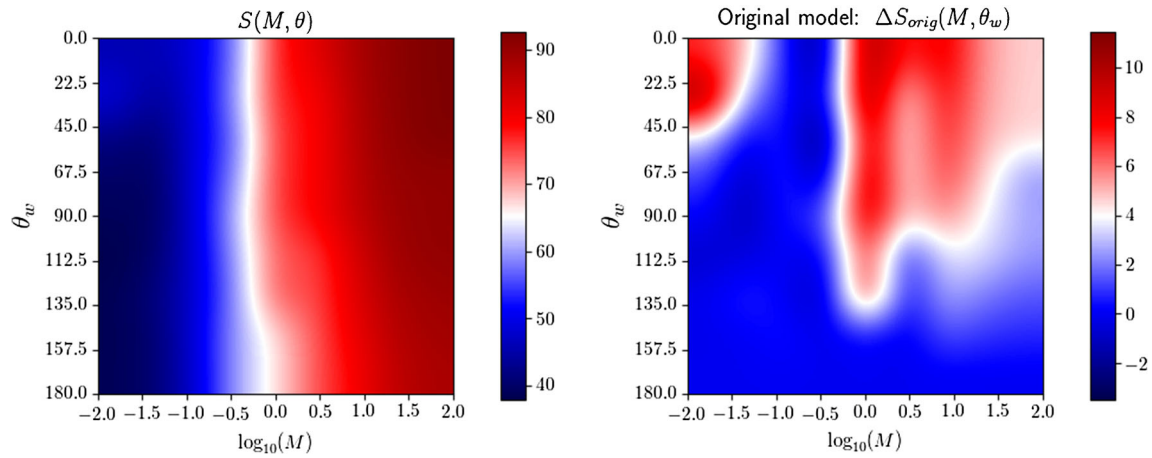

Fig. 3 Phase space showing the saturation at the moment of breakthrough as a function of viscosity ratio and wetting angle (left), and phase space showing the difference in the saturation at the moment of breakthrough as a function of viscosity ratio and wetting angle relative to the saturation at a wetting angle of $\theta_w = 180°$ (right). Calculations were made at a capillary number of $Ca \sim 5$ which is in the viscous fingering regime

case of $M = 1 \Rightarrow \nu_r = \nu_b = 0.2$, we will have an injection velocity of $u_{in} = 0.01$.

Flow patterns

We performed 81 simulations using the model shown in Fig. 1 spanning the space of ($M \in [0.01, 100], \theta_w \in [0°, 180°]$) where we sample M in increments of $\Delta \log_{10} M = 0.5$ and θ_w in increments of $\Delta\theta_w = 22.5°$.

Figure 2 shows snapshots of the fluid flow at the time of breakthrough when the red fluid reaches the right boundary of the model for various M and θ_w. These plots indicate that as expected, low viscosity ratios lead to patterns of narrow tendrils of the red fluid (shown as black) invading the blue fluid (shown as white)—i.e., viscous fingering—leading to low saturation, whereas for high viscosity ratios we see a distorted almost linear front of the invading fluid—i.e., stable displacement—leading to higher saturation.

Figure 2 shows a different morphology of fingers of the wetting and non-wetting cases at a viscosity ratio $M = 0.01$ where viscous fingering is strongest. Namely, the fingers for the wetting case ($\theta_w = 0°$) are broader and more rounded than the fingers for non-wetting case ($\theta_w = 180°$) suggesting increased saturation with wettability. This is consistent with theoretical and experimental studies (Stokes et al. 1986; Trojer et al. 2015; Zhao et al. 2016; Primkulov et al. 2019).

Phase space study

Figure 3 shows the phase space of saturation as a function of M and θ_w at breakthrough denoted $S(M, \theta_w)$ and the phase space of saturation difference $\Delta S(M, \theta_w) = S(M, \theta_w) - S(M, 180°)$ which highlights the effect of wetting angle on saturation at a given M. These phase spaces compile the saturation at breakthrough and saturation difference at breakthrough results of the 81 simulations spanning $M \in [0.01, 100]$ and $\theta_w \in [0°, 180°]$.

We observe that on the plot of the saturation phase space that—as expected—the dominant effect is the viscosity ratio with higher saturation as the viscosity ratio increases. The saturation difference phase space which highlights the effect of wettability shows a more complicated pattern. Although there is some tendency for saturation to increase as wettability increases, the phase space landscape has a complex shape with a hill at ($M = 0.01, \theta_w = 22.5°$), a

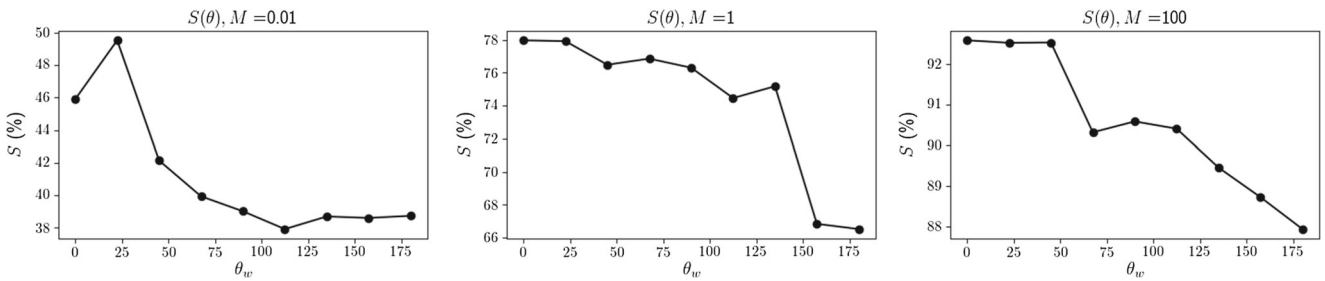

Fig. 4 Plots of the saturation versus wetting angle at breakthrough for viscosity ratios of $M = 0.01$ (left), $M = 1$ (center), and $M = 100$ (right)

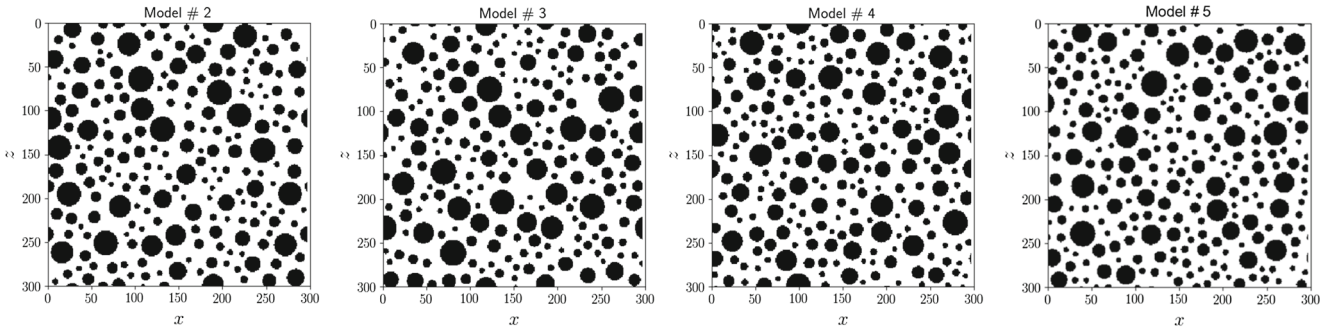

Fig. 5 Four additional random model realizations that were created using the same algorithm and input parameters were used to generate the original model (model 1)

valley with no significant effect on saturation at $\log_{10} M \in [-1, -0.5]$, a ridge at $M = 1$ where saturation tends to be higher for more wetting fluids, and a ridge and plateau at $\log_{10} M \geq 1$.

Figure 4 shows profiles of saturation versus wetting angle for $M = 0.01$, $M = 1$ and $M = 100$ and details the shape of the hill at $M = 0.01$ and the ridge at $M = 1$. The increase in saturation with wettability up until an optimal angle of $\theta_w = 22.5°$ for the case of $M = 0.01$ is consistent with microfluidic experiments of Zhao et al. (2016) involving flow through vertical posts representing a porous medium. In their work, they found that as wettability is increased,

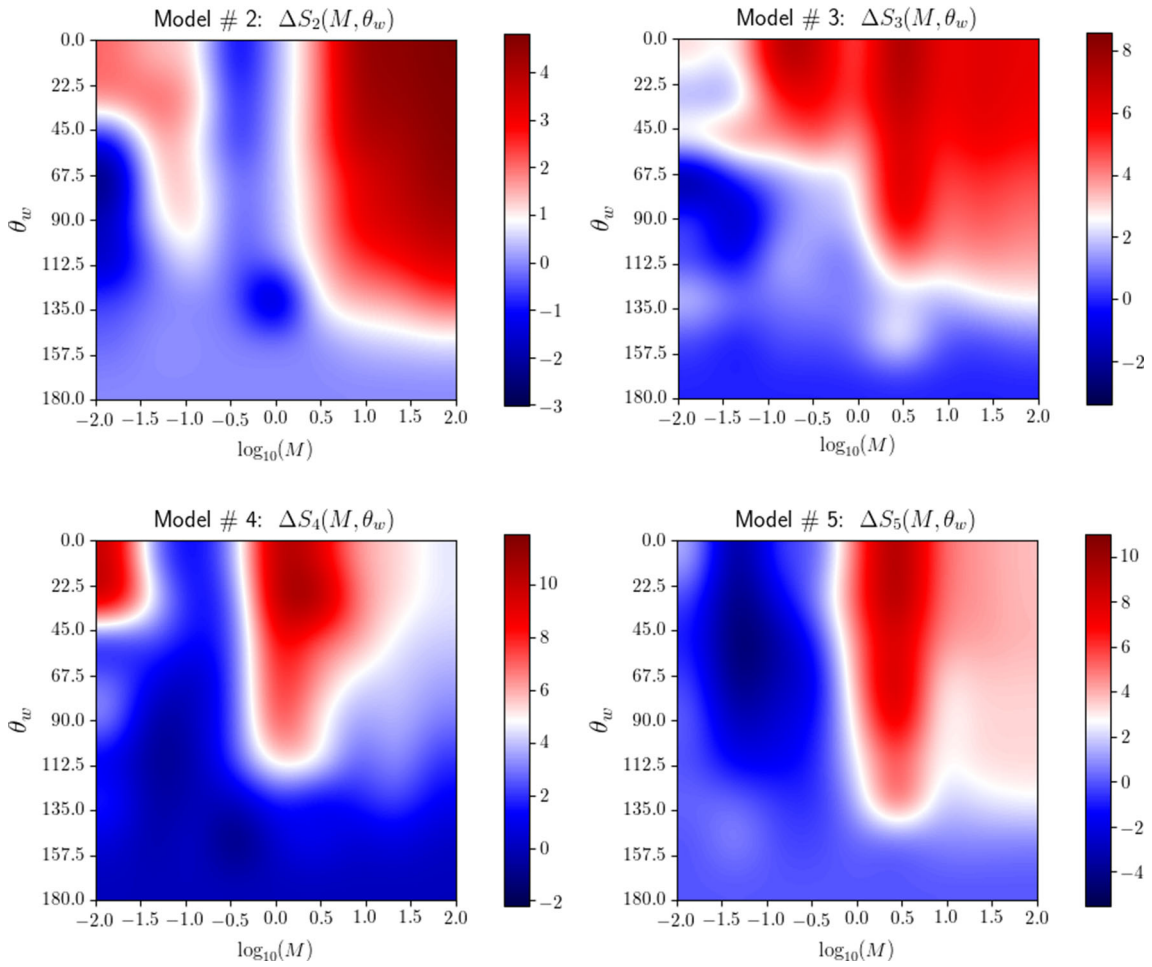

Fig. 6 Plots of the phase space of the difference in saturation $\Delta S(M, \theta_w)$ for the suites with the 10 different random model realizations. The plots are ordered such that similar phase space topographies are adjacent to one another. Calculations were made at a capillary number of $Ca \sim 5$ which is in the viscous fingering regime

there is more efficient displacement and higher saturation up until a critical angle is reached, after which, the system undergoes a wetting transition and the trend is reversed.

Sensitivity to porous model structure

To study the effect of the porous model on the phase space difference which captures the wetting angle effect, we ran suites for ten more random models, bringing the total number of suites run to 11. As the model size is small, these can be considered as different models rather than different random realizations of the same model. Figure 5 shows four of these additional random models and Fig. 6 shows the corresponding phase space difference plots. These four suites were chosen as their phase space difference plots together with the plot shown in Fig. 3 capture typical features of the phase space landscapes of the eleven runs. Namely, we observe that while there is some tendency for saturation to be higher for more wetting fluids, these plots are all different and have a complex landscape with feature such as hills, valleys, ridges, and plateaus. This suggests (1) the possibility that there may be specific wetting angles not necessarily $\theta_w = 0°$ which maximize saturation at a given viscosity ratio for a given porous rock matrix, and (2) that at some viscosity ratios there may be only a negligible effect of wetting angle on saturation.

For example, for the original model as shown in Fig. 3, there was an optimal wetting angle that maximized saturation at $\theta_w = 22.5°$ for $M = 0.01$, which is also apparent for models 2 and 4 as shown in Fig. 6, whereas for models 3 and 5, there is a minor or even negative correlation with saturation on wettability at $M = 0.01$. Also, for models 2 and 3, one observes that the saturation is maximized at around $\theta_w \sim 34°$ and $\theta_w \sim 45°$ for $M = 0.1$ and $M = 0.03$, respectively, which is not the case for the other two models which have no wetting effect or a negative correlation of saturation with wettability at this viscosity ratio.

Post-breakthrough flow and saturation evolution

For the case of the original model, we also did runs well beyond breakthrough for the wetting and non-wetting cases

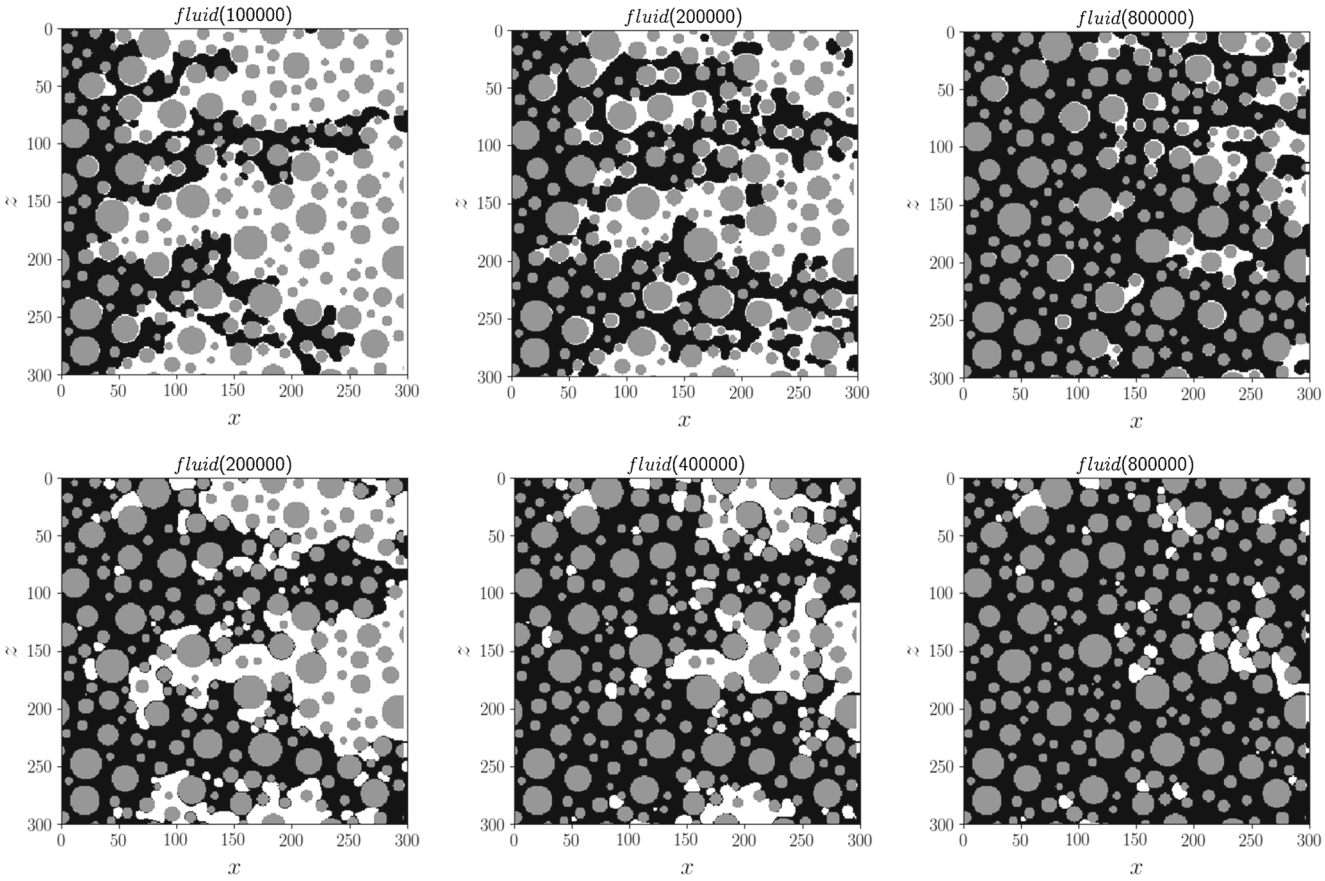

Fig. 7 Snapshots showing the evolution of fluid displacement with time after breakthrough for a viscosity ratio of $M = 0.01$ (top row: non-wetting invading fluid at times of 100,000, 200,000, and 800,000 units of time; bottom row: wetting invading fluid at times of 200,000, 400,000, and 800,000 units of time)

at the lowest viscosity ratio of $M = 0.01$. Figure 7 shows snapshots of the flow evolution at several times after breakthrough and Fig. 8 shows the fluid flow velocity field at the same times. From these plots, it is clear that the flow field is not static after breakthrough, but the fingers continue to evolve and expand. After 1,000,000 time steps which is of order ten times the breakthrough time, the model is almost 100% saturated.

Figure 9 shows saturation as a function of time up to and beyond breakthrough and indicates that for a constant rate of injection, the saturation increases with time for both non-wetting and wetting cases are similar. The fully wetting case reaches a higher saturation at breakthrough but at a later time than the non-wetting case. What is most interesting is that beyond breakthrough, the saturation continues to increase albeit at a slower rate for both the wetting and non-wetting cases. Immediately after breakthrough, the rate of saturation increase drops by about a factor of 2 and successively slows as time proceeds. At about 10 times the breakthrough time, the saturations for both wetting and non-wetting cases are around 90%.

Discussion

The results suggest that the saturation at breakthrough or recovery factor is a complicated function of viscosity ratio, wetting angle, and the porous rock structure. Specifically, oil recovery by water flooding of a specific oil field—and hence viscosity ratio—may be optimal at a specific wetting angle rather than for a fully wetting fluid. Furthermore, the results show that the saturation does not stop increasing at breakthrough. Instead, the fingers continue to evolve and grow, and eventually, the saturation for both wetting and non-wetting cases is around 90% at about ten times the breakthrough time. This suggests that with a long enough time, very high production rates of order 90% production of a specific oil field may be possible. Even if this result is verified, economic factors related to the cost of continued water flooding for a long time will play the key role in regard to the extent an oil field may be produced.

Finally, the rate of saturation increase is similar for both wetting and non-wetting fluids at a given injection rate suggesting that similar productivity of a given well may be

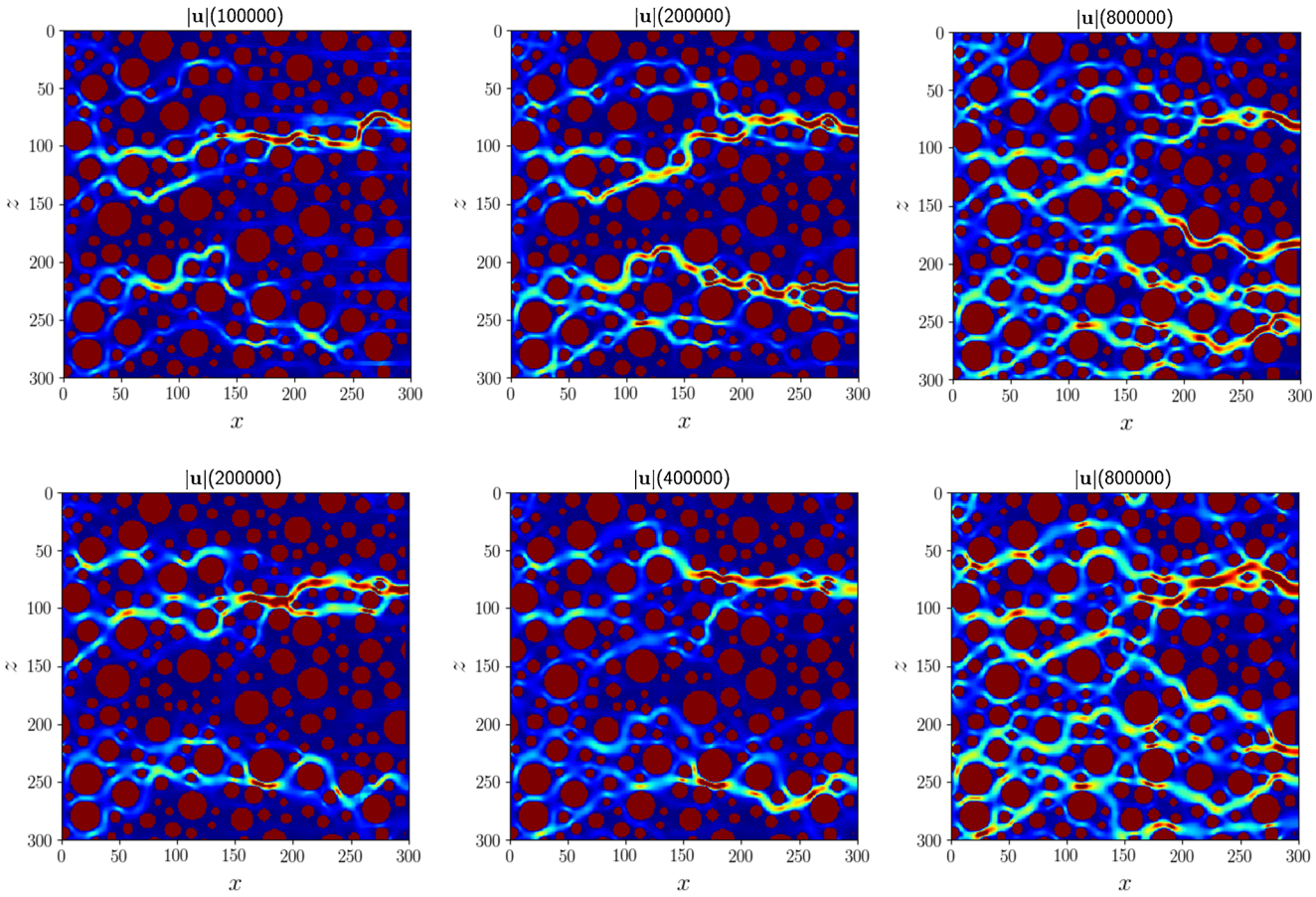

Fig. 8 Snapshots showing the evolution of fluid velocity with time after breakthrough for a viscosity ratio of $M = 0.01$ (top row: non-wetting invading fluid at times of 100,000, 200,000, and 800,000 units of time; bottom row: wetting invading fluid at times of 200,000, 400,000, and 800,000 units of time)

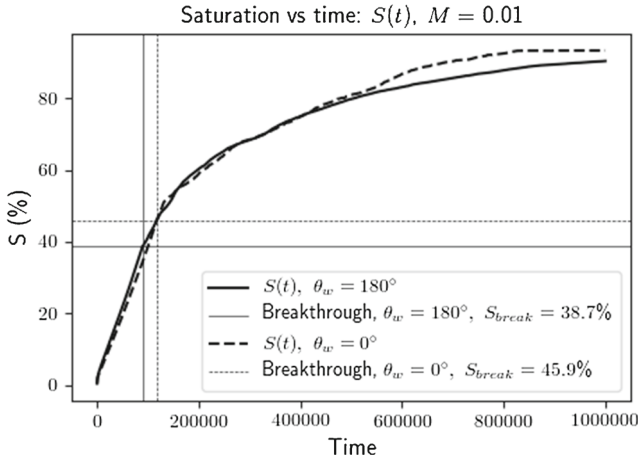

Fig. 9 Plot showing the evolution of the saturation through time for the original model before and after the moment of breakthrough for the case of viscosity ratio $M = 0.01$ and the non-wetting and perfectly wetting cases (i.e., wetting angles $\theta_w = 180°$ and $\theta_w = 0°$).

achieved independently of wettability. Namely, although the recovery factor may be higher for a more wetting invading fluid at breakthrough, this takes longer to achieve than for a non-wetting fluid. So if water flooding is done using a non-wetting injection fluid for a given time $\sim$ the time of breakthrough had a wetting fluid been used, the saturation and hence recovery factor should be similar.

Conclusions

We conducted suites of numerical experiments of two-phase flow through a simplified 2D porous rock matrix using the Rothman-Keller color gradient lattice Boltzmann method (LBM). These involved injecting red fluid from the left of five 2D porous medium models saturated with a blue fluid over a range of viscosity ratios $M \in [0.01, 100]$ and wetting angles $\theta_w \in [0°, 180°]$. The simulations show that the viscous fingering effect on saturation or recovery factor is complex. Specifically, we observe that while saturation at breakthrough has some broad tendency to increase with wettability, this is not always the case and the saturation landscape as a function of wettability and viscosity ratio can have hills and valleys which depend on the porous medium model. This suggests the possibility that optimal wetting angles exist for each viscosity ratio for a given model, such that saturation, and hence recovery factor, is maximized. Furthermore, the results show that the saturation does not stop increasing at breakthrough when the fingers have traversed the model. Instead, these fingers continue to evolve and grow, and eventually, the saturation for both wetting and non-wetting cases is around 90% at about ten times the breakthrough time. And finally, for a specified injection rate, the rate of saturation increase is similar for both wetting and non-wetting invading fluids up to and beyond breakthrough suggesting that the time of water flooding rather than wettability may be the main factor controlling ultimate production of a field using water flooding. Further research using large-scale 3D models and experimental studies are required to verify how our conclusions translate to the real world. Nonetheless, the results demonstrate the potential of the LBM to be used to study multiphase flow and viscous fingering phenomena, and to uncover unexpected behavior relevant to enhanced oil recovery (EOR). Ultimately, the LBM may prove to be a powerful tool to optimize EOR, when used in conjunction with experimental validation studies.

Funding This research was supported by the College of Petroleum Engineering and Geosciences at King Fahd University of Petroleum and Minerals, Saudi Arabia. In addition, this research was funded by the US Department of Energy Grant DE-SC0019759 (D.A.Y.) by the National Science Foundation (NSF) Grant EAR-1918126 (D.A.Y).

Declarations

Conflict of interest The authors declare that they have no competing interests.

References

Chen S, Doolen G (1998) Lattice Boltzmann method for fluid flows. Annu Rev Fluid Mech 30:329–364

Chen JD, Wilkinson D (1985) Pore–scale viscous fingering in porous media. Phys Rev Lett 55(18):1892–1896

Deng X, Kamal MS, Patil S, Hussain SMS, Zhou X (2020) A review on wettability alteration in catbonate rocks: wettability modifiers. Energy and Fuels 34:31–54

Grunau D, Chen S, Eggert K (1993) A lattice Boltzmann model for multiphase fluid flows. Physics of Fluids A: Fluid Dyanmics 5(10):2557–2562

Gunstensen AK, Rothman DH, Zeleski S, Zanetti G (1991) Lattice Boltzmann model of immiscible fluids. Phys Rev A 43(8):4320–4327

Homsy GM (1997) Viscous fingering in porous media. Ann Rev Fluid Mech 19:271–311

Huang HB, Huang JJ, Lu XY (2014) Study of immiscible displacements in porous media using a color-gradient-based multiphase lattice Boltzmann method. Comput Fluids 93:164–172

Huang HB, Sukop M, Lu XY (2015) Multiphase lattice Boltzmann methods: Theory and application (chapter 4). Wiley

Jadhunandan PP, Morrow NR (1995) Effect of wettability on waterflood recovery for crude-oil/brine/rock systems. SPE Reserv Eng 10:40–46

Kennedy HT, Burja EO, Boykin RS (1955) An investigation of the effects of wettability on the recovery of oil by water flooding. J Phys Chem 59:867–879

Latva-Kokko M, Rothman D (2005) Static contact angle in lattice Boltzmann models of immiscible fluids. Phys Rev E 74(4):046701

Lenormand R, Touboul E, Zarcone C (1988) Numerical models and experiments on immiscible displacements in porous media. J Fluid Mech 1989:165–187

Mora P, Morra G, Yuen D (2021) Optimal surface tension isotropy in the Rothman-Keller colour gradient Lattice Boltzmann

Method for multi-phase flow. Phys Rev E 103(3):033302. https://doi.org/10.1103/PhysRevE.103.033302
Mora P, Morra G, Yuen D, Juanes R (2021) Optimal wetting angles in Lattice Boltzmann simulations of viscous fingering. Flow in Porous Media 136:831–842. https://doi.org/10.1007/s11242-020-01541-7
Morrow N, Buckley J (2011) Improved oil recovery by low salinity waterflooding. J Pet Technol 63:106–112
Måløy KJ, Feder J, Jøssang T (1985) Viscous fingering fractals in porous media. Phys Rev Lett 55(24):2688–2691
Primkulov BK, Pahlavan AA, Fu X, Zhao B, Macminn CW, Juanes R (2019) Signatures of fluid-fluid displacement in porous media: wettabilities, patterns and pressures. J Fluid Mech 875:R4
Qian Y, d'Humières D, Lallemand P (1992) Lattice BGK models for Navier-Stokes equation. Europhysics Lett 17(6):479. http://stacks.iop.org/0295-5075/17/i=6/a=001
Reis T, Phillips TN (2007) 2007 Lattice Boltzmann model for simulating immiscible two-phase flows. J Phys A Math Theor 40(14):4033–4053
Rothman D, Keller J (1988) Immiscible cellular automaton fluids. J Stat Phys 52(3/4):1119–1127
Seethepalli A, Adibhatla B, Mohanty KK (2004) Physicochemical interactions during surfactant flooding of fractured carbonate reservoirs. SPE J 9(4):411–418. https://doi.org/10.2118/89423-PA
Sharma G, Mohanty KK (2013) Wettability alteration in high-temperature and high-salinity carbonate reservoirs. SPE J 18(04):646–655
Stokes JP, Weitz DA, Gollub JP, Dougherty A, Robbins MO, Chaikin PM, Lindsay HM (1986) Interfacial stability of immiscible displacement in a porous medium. Phys Rev Lett 57(14):1718–1721
Trojer M, Szulczewski ML, Juanes R (2015) Stabilizing fluid–fluid displacements in porous media through wettability alteration. Phys Rev Appl 3(5):054008
Zhao B, MacMinn CW, Juanes R (2016) Wettability control on multiphase flow in patterned microfluidics. Proc Natl Acad Sci USA 113(37):10251–10256
Zhao B, MacMinn CW, Primkulov BK, Chen Y, Valocchi AJ, Zhao J, Kang Q, Bruning K, McClure JE, Miller CT, Fakhari A, Bolster D, Hiller T, Brinkmann M, Cueto-Felgueroso L, Cogswell DA, Verma R, Prodanovic M, Maes J, Geiger S, Vassvik M, Hansen A, Segre E, Holtzman R, Yang Z, Yuan C, Chareyre B, Juanes R (2019) Comprehensive comparison of pore-scale models for multiphase flow in porous media. Proc Natl Acad Sci U.S.A 120:13799–13806
Zou Q, He X (1997) On pressure and velocity flow boundary conditions and bounce back for the lattice Boltzmann BGK model. Phys Fluids 9:1591–1598

Affiliations

Peter Mora[1] · Gabriele Morra[2] · Dave A. Yuen[3,4] · Ruben Juanes[5]

Gabriele Morra
morra@louisiana.edu

Dave A. Yuen
daveyuen@gmail.com

Ruben Juanes
juanes@mit.edu

1 College of Petroleum Engineering and Geosciences, King Fahd University of Petroleum and Minerals, Dhahran, 31261, Saudi Arabia

2 Department of Physics, University of Louisiana at Lafayette, 104 E University Ave, Lafayette, LA 70504, USA

3 Department of Applied Physics and Applied Mathematics, Columbia University, New York, NY 10027, USA

4 Department of Information Science and Engineering and College of Marine Geosciences, Ocean University of China, 238 Songling Road, Qingdao, 266100, China

5 Department of Civil and Environmental Engineering, Massachusetts Institute of Technology, Cambridge, MA 02139, USA